

Master's thesis to obtain the INSA Engineering degree in Topography



---

## Acquisition and Processing Protocols for UAV Images 3D Modeling of Historical Buildings using Photogrammetry

---

*(abridged and translated from the French version)*

Presented on September 21<sup>st</sup> 2016 by Arnadi Murtiyoso

*Host company:*

Drone Alsace  
4 Rue Sainte Catherine  
67000 Strasbourg, France  
[www.drone-alsace.fr](http://www.drone-alsace.fr)

*In collaboration with:*

ICube Laboratory UMR 7357  
Photogrammetry and Geomatics Group  
INSA de Strasbourg  
24 Boulevard de la Victoire  
67084 Strasbourg, France  
[icube-trio.unistra.fr](http://icube-trio.unistra.fr)

*Thesis director:*

Tristan Freville (Drone Alsace, Manager)

*Supervisors and examiners:*

Mathieu Koehl (INSA de Strasbourg, Associate Professor)  
Pierre Grussenmeyer (INSA de Strasbourg, Professor)

## Abstract

The use of image-based techniques to document heritage sites has seen resurgence in recent years with advancements in optical sensors as well as computing power. The rise of UAVs (Unmanned Aerial Vehicles) also complements this technique, by providing the advantage of aerial view over traditional terrestrial image acquisition. Recently UAVs began to become more and more specialized towards specific tasks, 3D modeling and reconstruction being some of them. In this study the use of state of the art UAV dedicated for close range inspection is analyzed. Several case studies were performed on historical buildings in Strasbourg, France. A preliminary test was performed on the Joséphine Pavillion, while two case studies were conducted on the Rohan Palace and the St-Pierre-le-Jeune Catholic church. In the case of the church, data from two different UAVs as well as terrestrial images were combined. Processing was then done by utilizing both commercial and open source photogrammetry and SfM (Structure from Motion) solutions. Both the quality of the aerotriangulation and the dense matching were studied. In addition, the palace and the church were scanned using a laser scanner. This data is then used as references in comparing the results of the photogrammetric dense matching. Results show a centimetric precision in all cases, while highlighting some problems with the quality of images. The final objective of this project is to adapt existing terrestrial image acquisition and processing protocols for use by UAVs.

**Keywords:** UAV, documentation, photogrammetry, close range, protocols, heritage buildings.

## Table of contents

|  |    |
|--|----|
| Abstract.....  | 2  |
| Table of contents .....  | 3  |
| Table of figures .....   | 4  |
| Chapter I    Introduction .....  | 5  |
| Chapter II   State of the Art.....   | 7  |
| II.1    About UAVs.....  | 7  |
| II.2    Existing image acquisition and processing protocols .....          | 7  |
| II.3    Legal requirements for UAV flights.....                            | 7  |
| II.4    Image matching algorithms .....                                    | 8  |
| II.5    Software solutions .....   | 9  |
| Chapter III   Tools and methods.....                                       | 10 |
| III.1    Tools.....  | 10 |
| III.1.1    UAVs.....   | 10 |
| III.1.2    Terrestrial instruments .....                                   | 10 |
| III.1.3    Documentations.....   | 11 |
| III.2    Methods.....  | 11 |
| III.2.1    Acquisition methods .....                                       | 11 |
| III.2.2    Processing methods .....  | 11 |
| III.2.3    Theoretical precision for the aerotriangulation.....            | 12 |
| III.2.4    Estimated resolution of dense point cloud.....                  | 12 |
| Chapter IV   Results and analysis .....                                    | 14 |
| IV.1    Sensor calibrations.....   | 14 |
| IV.2    Preliminary test: the Joséphine Pavilion.....                      | 15 |
| IV.3    First case study: the Rohan Palace.....                            | 16 |
| IV.4    Second case study: the Saint-Pierre-le-Jeune Catholic church ..... | 19 |
| Chapter V    Conclusions .....   | 23 |
| References cited in this translation .....                                 | 25 |

## Table of figures

|  |    |
|--|----|
| Figure I.1 The different aspects of the project. ....  | 5  |
| Figure II.1 General classification of image matching methods, adapted from (Szeliski 2010; Remondino et al. 2013; Remondino et al. 2014) .....   | 8  |
| Figure III.1 The UAV used in the study, Sensefly Albris and DJI Phantom 3 Professional as well as the main characteristics of their respective platforms and on board cameras. ....  | 10 |
| Figure III.2 Combination of perpendicular and oblique flights for façade acquisition. ....   | 11 |
| Figure III.3 Illustration of the project decomposition principle used in this study. ....  | 11 |
| Figure IV.1 Dense matching results of the central front-façade of the Josephine Pavilion, showing point clouds generated by the five dense matching algorithms employed. ....  | 15 |
| Figure IV.2. Dense point cloud generation parameters of the four algorithms tested. ....   | 16 |
| Figure IV.3. Dense matching results analysis using laser scanning data as reference for a common part of the façade of the Rohan Palace. ....  | 17 |
| Figure IV.4. A horizontal profile of one of the Corinthian columns (red square) and a vertical one of a part of the wall (green square). The blue lines represent laser scanner measurements. ....                           | 18 |
| Figure IV.5. 3D meshed model of the St-Pierre data set and samples used to analyse the photogrammetric dense matching results. Blue frames indicate acquisition by Albris, while red indicate acquisition by Phantom 3. .... | 20 |
| Figure IV.6. Dense matching results analysis for the principal façade of the St-Pierre church. ....  | 21 |
| Figure IV.7. Dense matching results analysis for the central tympanum of the St-Pierre church. ....  | 21 |
| Figure IV.8. Dense matching results analysis for the southeastern portal of the St-Pierre church. ....   | 22 |
| Figure IV.9. Dense matching results analysis for the St. Matthew's gargoyle of the St-Pierre church. ....  | 22 |

## Chapter I Introduction

Aerial photography has a long history of applications in cartography. It has a very large range of applications and can be used to minimize work on the ground. Photogrammetry is a standard tool often used for large scale applications. This technique enables the user to obtain 3D data of the zone of interest, and eventually may also be used to produce orthophotos. Photogrammetry has also seen an increase in the use of UAVs (Unmanned Aerial Vehicles) for smaller scale cartography. The use of drone is also advantageous because it may be used for tasks requiring quick response, including in the case of the inspection and monitoring of building façades.

Originally a military conception, the UAV has seen a significant shift towards civilian use. The spread of UAVs complements the already existing terrestrial image based techniques, in enabling a close range aerial photogrammetry operation. Coupled with the developments in sensors as well as computing power, this type of surveying becomes a very powerful solution for various uses. Heritage documentation naturally benefits from these developments, as it complements terrestrial techniques (Nex & Remondino 2014). Some examples in this domain can be seen in the works of (Reich et al. 2012; Baiocchi et al. 2013; Achille et al. 2015; Alidoost & Arefi 2015).

In the remote sensing domain, the on-board sensor's optics play a significant role. Several UAV manufacturers have tried to integrate better quality lenses, but the payload remains an important issue. On the other hand, the field of computer vision has largely facilitated and complemented classical photogrammetry. As explained in (Remondino et al. 2012; Chiabrando et al. 2015), the typical workflow involves automatic tie point feature extraction and matching. This is often followed by robust outlier detection and elimination and bundle block adjustment in order to retrieve the position and orientation of each camera station (the external parameters).

The company Drone Alsace is a UAV operator and member of the French Professional Civil UAV Federation (*Fédération Professionnelle du Drone Civil/FPDC*) which works in the domain of geomatics, technical inspections as well as audiovisuals. Various UAVs are in its service, including a multi-rotor and fixed-wing UAV for applications in larger areas. Drone Alsace performs feasibility studies, from data acquisition up to processing and analysis. For this project, a UAV designed especially for industrial inspections was used (the Albris from Sensefly).

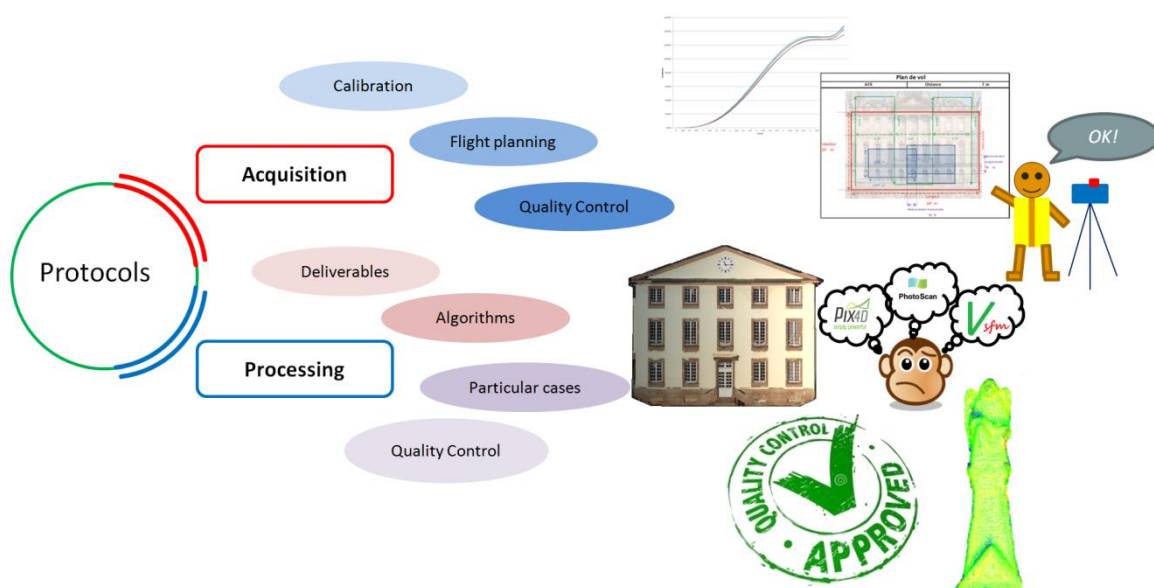


Figure I.1 The different aspects of the project.

The objective of the project is to study the acquisition and processing protocols which exist in the literature and to adapt them for UAV projects. This implies a study on the calibration of the sensors, flight planning, comparison of software solutions, 3D modeling of the objects, and analysis on the different products of a UAV project. Furthermore, a geometric and visual analysis of the results will be performed (Figure I.1).

The calibration of the sensor was performed using several softwares in order to compare the results. A dedicated calibration site was established within the INSA Strasbourg premises. This calibration site follows the recommendations of the various literatures. This fixed apparatus, complete with coded targets measured by a total station, will enable further calibrations to be performed in a rigorous fashion in the future.

As regards to the data acquisition, this project presents protocols to capture as much detail as possible. It is an implementation of images with large overlaps in the form of oblique images for building façades. This method enables the reconstruction of difficult angles and hidden areas which are normally difficult to capture using classical perpendicular flight plan. All flight planning are performed before the acquisition is performed, which reduces the time necessary in the field. Supporting documents were also created in order to document the mission as well as the object's metadata.

This study will also present a strategy for the processing of large numbers of images. The proposed method divides the images into clusters before fusing them in the end, after the meshing process. A radiometric compensation is then performed on the final unified model in order to generate a homogeneous 3D model.

Two historical buildings of the city of Strasbourg were used as case studies: a part of the Rohan Palace façade and the Saint-Pierre-le-Jeune Catholic church. The data acquisition was performed using the UAV photogrammetry technique and a terrestrial laser scanner was also employed to acquire reference data. These buildings were chosen with the recommendation of the Strasbourg City Council by taking into account the different challenges related to both the acquisition and the processing. It is also a pilot project for the 3D recording of historical buildings of the city of Strasbourg with the final objective of integrating them within the city's 3D GIS (Geographic Information System).

## Chapter II State of the Art

### II.1 About UAVs

Several categorizations of UAVs were given by (Fritsch et al. 2013; Remondino et al. 2011; Nex & Remondino 2014; Colomina & Molina 2014). A more practical classification of UAV types based on their physical structure can also be derived from these broad categorizations, as given by (Nex & Remondino 2014; Remondino et al. 2012; Achille et al. 2015) which divides it into three main categories:

1. Lighter than air platforms, such as balloons and kites. This category is low-cost but is more difficult to control due to its low wind resistance and low velocity.
2. Fixed-wing platforms, with the capability of covering a large surface but may be limited in payload as well as wind resistance. The fixed-wing UAV is suited for larger-scale mapping resembling classical small-format aerial photogrammetry.
3. Rotary-wing platforms, either with a single or multiple rotors. This type of UAV has a larger payload and wind resistance, but its surface coverage can be significantly lower than that of the fixed-wing type.

### II.2 Existing image acquisition and processing protocols

Several acquisition and processing procedures exist in the literature which deals mainly with terrestrial images. Often these protocols deal also with the calibration and other recommendations (project documentation, tips for radiometric calibration, object metadata, etc.) for facilitating later processing steps, up to the creation of a database. The CIPA Heritage Documentation's 3x3 rules have existed since 1994 with several updates (Grussenmeyer et al. 2002). The latest version can be consulted in the CIPA website (<http://cipa.icomos.org/>). Another protocol called TAPENADE (Tools and Acquisition Protocols for Enhancing Artifacts Documentation) was developed for the documentation of cultural heritage (Pierrot-Deseilligny et al. 2011; Nony et al. 2012). However, up until the writing of this article, only French versions of TAPENADE is available although a more general explanation of the recommendations in English is available in the website (<http://www.tapenade.gamsau.archi.fr/>). The University of Stuttgart's Institute for Photogrammetry has also developed their own protocol (Wenzel, Rothermel, Fritsch, et al. 2013) called "One panorama each step". It is targeted to produce a good dense matching result by using greatly overlapping images. This protocol has also been tested on UAV data.

These existing protocols share some similarities. First, a good calibration using a convergent, controlled environment is always recommended rather than relying solely on in situ self-calibration, a fact which is also corroborated by (Fraser 2013a; Hastedt & Luhmann 2015). The importance of procedural documentation and description of the object is also stressed, something which is sometimes forgotten but is nevertheless important. Finally, all three rules emphasize two kinds of image acquisition. The first involves general or global images with good convergence angles to ensure the geometric favorability of the resulting network while the second involves images with very large percentage of overlap (detailed stereo pairs) to facilitate the dense matching process.

### II.3 Legal requirements for UAV flights

Being an unmanned platform, the regulations for UAV often concern the security of citizens in the event of impact (Nex & Remondino 2014). A quick comparison of the legal requirements of UAV missions in certain countries are presented below (Morales et al. 2015), bearing in mind that these rules may evolve quickly.

1. *United States (US)*: In the US, UAV missions are controlled by the FAA (Federal Aviation Administration). For recreational use, the FAA only gives simple instructions of security which governs the maximum height of flight, visibility, distance of flight, and weight of the platform.
2. *Canada*: The situation in Canada is somewhat similar to France. Several flight scenarios exist which determines the type of permit required. However, a flight without permit is still possible under certain circumstances.
3. *Spain*: The use of UAVs in Spanish territory is limited to scientific, agricultural, and emergency related missions. A UAV pilot must be certified by the EASA (European Aviation Safety Agency).
4. *United Kingdom (UK)*: UAV in the UK is regulated by the CAA (Civil Aviation Authority). In general the rules are similar to other countries cited in this paragraph, notably concerning the visibility of the UAV. Images or videos containing information on other people's privacy are forbidden.
5. *France*: Permits pertaining to the use of UAVs are delivered by the French civil aviation agency (DGAC). Four flight scenarios are defined, which depends on the flight conditions and the nature of the platform (DGAC 2015).
6. *Indonesia*: At the moment of writing of this paper, only a ministerial decree has a legal power to regulate the flight of drones in Indonesia (Kemenhub 2015), as no laws regarding this matter has been passed yet.

## II.4 Image matching algorithms

Most 3D reconstruction software which is based on images has their own algorithm for the generation of a dense point cloud. (Remondino et al. 2013) and more recently (Remondino et al. 2014) have tried to classify the different existing approaches to dense matching. The most basic classification is between the matching of features (i.e. comparison of descriptors) and the matching of grayscale value within a set search window. Once the correspondence is done, a simple mathematical calculation is performed in order to determine the coordinates of the object on the object space. The matching of features is otherwise called feature-based matching (FBM) while the other classification is called area-based matching (ABM) (Remondino et al. 2013).

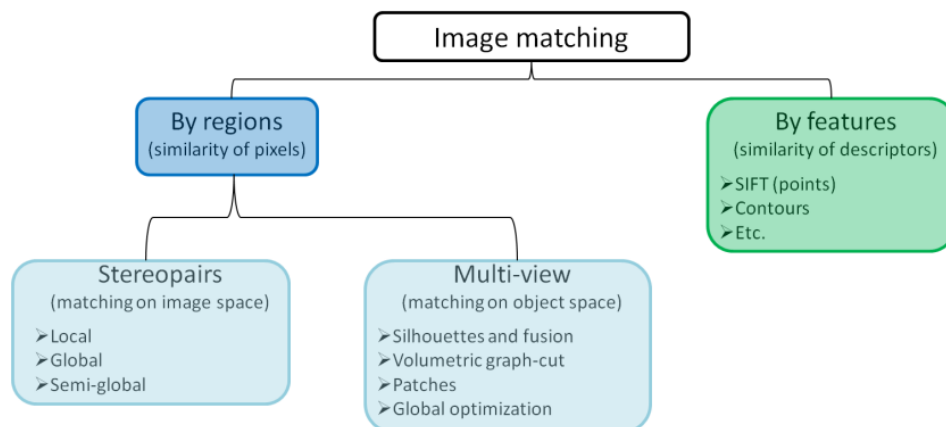


Figure II.1 General classification of image matching methods, adapted from (Szeliski 2010; Remondino et al. 2013; Remondino et al. 2014)

Algorithms which follow the ABM classification are very powerful, with the possibility to reach a matching precision of up to 1/50 pixels. However, ABM requires objects with textures as well as approximate values. On the other hand, FBM is less dependent on textures, even though the resulting point cloud is often not dense enough. Examples of FBM algorithms include SIFT (Lowe 2004), SURF (Bay et al. 2006), Harris detectors (Harris & Stephens 1988), etc.

FBM is often used to generate in the first place a sparse point cloud (Szeliski 2010). This sparse point cloud can be then used as approximate values for the dense matching stage which employs ABM. As



regards to ABM, two sub-categories exist which depend on the space where the matching is performed. The first one uses epipolar lines and therefore performs the matching in the image space. (Szeliski 2010) divided this approach into local and global methods. In the local method (based on a search window), the disparity or parallax for each pixel is calculated. The use of a window implies a smoothing on object borders (Hirschmüller 2011). The global method on the other hand, calculates an energy minimization on the entirety of the image with an explicit smoothing. Another method called the Semi-Global Matching (SGM) was proposed by (Hirschmüller 2005), in which an energy minimization on the length of the epipolar line is calculated, as well as other directions around the pixel.

The other sub-category of ABM performs the matching in the object space. In this approach, a sparse point cloud is necessary as approximate values in the matching process which may be obtained from an FBM matching. When such point cloud is available, the algorithm classifies the images according to their positions relative to the object to be reconstructed. Afterwards the dense matching is performed on a patch around a 3D point of the sparse point cloud seen by a certain group of images. This patch is then enlarged iteratively towards the neighboring pixels in the image space. A visibility constraint is added to filter the result of this matching (Furukawa & Ponce 2009). A diagram explaining this classification is shown in Figure II.1.

## II.5 Software solutions

Pix4D and Photoscan are two commercial solutions with a rather black-box nature. However, concurrent with the results of (Remondino et al. 2014), Photoscan most probably performs a modified SGM (Semi-Global Matching) (Hirschmüller 2011) of stereo pairs to generate depth maps, and then employs epipolar constraints at the end of this process to filter the results. Pix4D may have used a similar albeit different approach, since an SGM-based matching is offered as an additional plug-in.

Photomodeler has long been used by the architecture and archeology community for performing 3D image-based measurements (Grussenmeyer et al. 2002). This software has an advantage over other commercial solutions in that it provides more statistical information on its results, making it less black-box like. Photomodeler has since added a dense matching module based on stereo-pairs and more recently on a multi-view geometry.

The approach taken by SURE is well described in (Wenzel, Rothermel, Haala, et al. 2013). This software also uses a modified version of the SGM and computes a disparity map for each potential pair of images with a set value of overlap. The resulting depth-maps are then converted into a point cloud by employing geometric constraints to help reduce the number of outliers (Remondino et al. 2014). A free version of SURE is available for research or academic purposes.

Meanwhile, Micmac uses a multi-resolution and multi-image approach to dense matching (Pierrot-Deseilligny & Paparoditis 2006). The Micmac suite is modular and works with several levels of complexity and automation. The first module, Pastis, searches and matches tie points on the images. Aperio performs bundle block adjustment to retrieve the external orientation parameters of the camera stations. Finally, Micmac performs a pyramidal processing to search pixel correspondences. Results from a lower resolution matching are used to guide the matching at the higher resolution level, with the maximum resolution determined by a parameter (Remondino et al. 2014).

PMVS (patch-based multi-view stereo) uses a different object-based approach (Furukawa & Ponce 2009). It implements multi-view stereo-matching starting on a sparse point cloud generated by the SfM matched tie points. The matched “patch” around a tie point is then repeatedly expanded to nearby pixels and filtered using visibility constraints.

## Chapter III Tools and methods

### III.1 Tools

#### III.1.1 UAVs

The first UAV used in this project is a multi-copter rotary wing platform manufactured by the company Sensefly and called Albris since April 2016 (previously known as Exom). The product first appeared in the market in May 2015 and was aimed to perform close-range high resolution inspections, mapping, and 3D modeling. It is equipped with multiple sensors, including a still 38 megapixels camera, a thermal and a video camera. Several ultrasonic sensors give an approximate distance measurement of its surroundings, enabling it to fly on a set distance from an object. The still camera itself is furnished with an 8 mm lens and a 10 x 7.5 mm sensor. This specification theoretically enables a GSD (Ground Sampling Distance) of up to 1 mm at a distance of 6 meters.

Another UAV used is the DJI Phantom 3 Professional, also a multi-copter rotary wing type. This UAV was first released also in May 2015. The Phantom 3 is lightweight and relatively low-cost, but it is not geared for dedicated close-range inspection tasks. Unlike the previous versions, the Phantom 3 is no longer equipped with a fish-eye lens camera. This could potentially yield a better geometric result, but the sensor itself remains very small compared to most terrestrial cameras. It is equipped with a 4 mm lens and a 6.5 x 5 mm sensor. Figure III.1 shows the main characteristics of these two UAVs.



| Sensefly Albris |                    |
|-----------------|--------------------|
| Platform        |                    |
| Payload         | 1.8 kg             |
| Flight autonomy | ~22 minutes        |
| Camera          |                    |
| Focal length    | 8 mm               |
| Sensor size     | 10 x 7.5 mm        |
|                 | 7152 x 5368 pixels |
| Horizontal FOV  | 63°                |



| DJI Phantom 3 Professional |                    |
|----------------------------|--------------------|
| Platform                   |                    |
| Payload                    | 1.3 kg             |
| Flight autonomy            | ~23 minutes        |
| Camera                     |                    |
| Focal length               | 4 mm               |
| Sensor size                | 6.5 x 5 mm         |
|                            | 4000 x 3000 pixels |
| Horizontal FOV             | 94°                |

Figure III.1 The UAV used in the study, Sensefly Albris and DJI Phantom 3 Professional as well as the main characteristics of their respective platforms and on board cameras.

#### III.1.2 Terrestrial instruments

Although the UAV is used extensively in this project to acquire images, several terrestrial images were nonetheless required to be taken. This is the case when there are vegetations around the object. In this project, the area around the Rohan Palace is clear from any obstacles. However, the Saint-Pierre-le-Jeune church is surrounded by trees. In order to cover the parts of the building hidden by the vegetation, terrestrial images were also taken and integrated within the photogrammetric project. In this case, a Nikon D3200 with a 24 mm focal was used.

A laser scanner was also used to acquire a point cloud of both objects. In this case the phase-based terrestrial laser scanner FARO Focus 3D X330 was used. The scanner is associated with the software

Faro Scene which performs the point cloud registration and georeferencing. The registration process may be aided by the use of spheres which are automatically detected in Scene. However, a manual registration of the point clouds is also possible.

### III.1.3 Documentations

Following the existing protocols, several procedural rules were established in order to document each UAV project. A metadata form was prepared to record the object's attributes, which enables the object to be eventually integrated in a database. Another form was also prepared which documents the process of data acquisition on the field. A spreadsheet file was also created which enables a semi-automatic flight planning calculations.

## III.2 Methods

### III.2.1 Acquisition methods

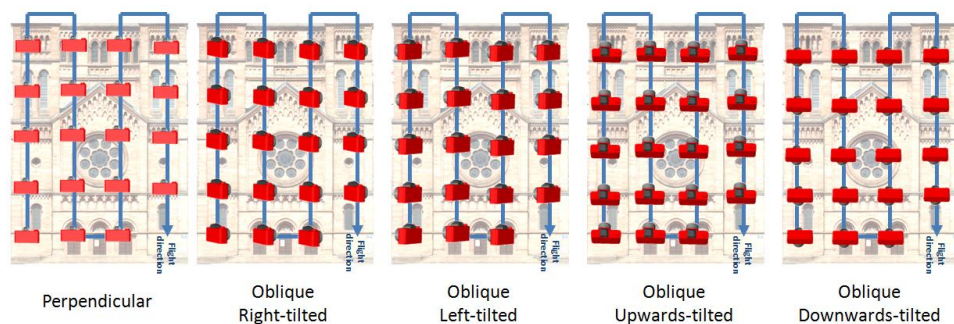


Figure III.2 Combination of perpendicular and oblique flights for façade acquisition.

In order not only to strengthen the image network geometry but also to better cover hidden parts, a flight taking perpendicular images was immediately followed by four oblique flights with the cameras tilted to the right, left, up, and down (Figure III.2).

The configuration of flight was not changed for all five flights in order to emulate a highly overlapping and convergent geometry. The primary downfall of this method is that the same flight must be performed five times for the five sensor positions. This increases flight time and therefore also poses problems in regards to battery issues and image texture homogeneity.

### III.2.2 Processing methods

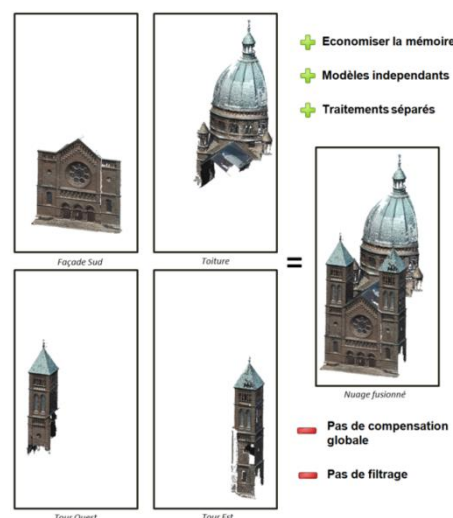


Figure III.3 Illustration of the project decomposition principle used in this study.

In principle, the photogrammetric workflow starts with the feature matching and followed by external orientation (and absolute orientation included) and dense matching based on the pixels. Indeed, in many software packages this workflow is already well defined. The user can generate the products simply by following the workflow given by the software developer. Often times, the user of open source softwares are directed towards forums or a community of users in which questions, responses, and information regarding the software can be found.

However, in the case of a project with large number of images (1000+), a form of project management is in order. A simultaneous processing of all images will require large amounts of resources (processor, memory, etc.). The strategy proposed in this study was used in the processing of the Saint-Pierre-le-Jeune dataset, which has more than 2500 images.

In this method, the project is divided into several smaller clusters. The proposed processing strategy is quite simple and follows the illustration given in Figure III.3. This decomposition has the advantage of facilitating the management of processing resources and also enables the project to advance in parallel with the data acquisition in the field. Therefore the clusters can be processed individually without having to wait until data acquisition is finished. However, this strategy does not permit the use of a global adjustment of the whole project. Moreover the generated point cloud is not filtered, which may result in redundant points. The radiometric adjustment is performed after the point clouds are assembled and meshed, as to render a smoother texture.

### III.2.3 Theoretical precision for the aerotriangulation

Historically, the theoretical estimation of aerotriangulation precision is determined by empirical formulas arising from the photogrammetry domain. A good example of this approach is elaborated by (Kraus & Waldhäusl 1998). In the advent of digital photogrammetry, the calculations must take into account several new parameters such as the GSD of the sensor.

The average GSD gives us a preliminary idea to the expected precision of a photogrammetric project (however the GSD can be very variable in close range photogrammetry), but manual measurement of control points can actually reach a sub-pixel level. (Gülch 1995) claimed that an experienced photogrammetrist is able to measure a manual point up to 0.13 pixels. However, (Kraus & Waldhäusl 1998) and more recently (Afsharnia et al. 2015) gave a more modest value of 0.3 pixels. Note that this value was used for metric cameras. In this case, where non-metric, small, and sometimes unstable sensors were used, a security coefficient of 2 may be added in order to take into account sensor instability, image noise, image compression, etc. Such practice of introducing security coefficients was also performed by (Kraus & Waldhäusl 1998). The formula used to calculate the theoretical aerotriangulation precision is therefore given in equation (1), where  $\sigma_{xyz}$  denotes the theoretical precision to be estimated.

$$\sigma_{xyz} = 0.3 * GSD * 2 \quad (1)$$

### III.2.4 Estimated resolution of dense point cloud

In the interest of estimating the theoretical resolution of photogrammetric dense point cloud, several common parameters between the different software solutions were identified. These parameters are non-exhaustive; it is merely the four most common parameters which are found in the majority of dense matching solutions. Even within the limits of these four parameters, their proper definition according to each algorithm may be different, which complicates the effort to compare them. These parameters are:

1. Pyramid level of the input images (P): The majority of software solutions offer the possibility to reduce the resolution of the input images for the dense matching process by means of image downsampling. It serves as a compromise between quality of the point cloud (i.e.

density) and processing time, which is often left to the user's choice. This parameter may go usually from 1 (i.e. full resolution) up to 0.03125 (i.e. 1/32 of the original resolution).

2. Downsampling rate (D): In the end of a dense matching process, the resulting point cloud is often too dense. Several software solutions offer the possibility to reduce the density by limiting the number of points generated. For example, a D equal to 4 means that one point will be matched for each 4 pixels of the image. This coefficient may go from 1 (no downsampling) up to 16 or more.
3. Point cloud filtering: Within each algorithm, the matching is performed in an iterative manner. In the stereopair-based approach, a point cloud is created for each stereopair and a point cloud filtering performed in the end, often using epipolar constraints. In approaches which select master and slave images, the filtering is performed before the matching. In the object space-based approaches, the filtering is performed based on visibility constraints.
4. Correlation coefficient threshold: This value determines the reliability of matched points. When this value is high, more points are generated. However, a higher value risks the generation of more noises. With a lower correlation coefficient, the results are filtered in a more rigorous manner. Less noise is therefore detected, but this may also reduce the number of points in the resulting point cloud. In certain commercial software such as Photoscan and Pix4D, this parameter is predefined. Micmac and Photomodeler users can modify this value manually.

From these parameters, estimation for the resolution of the dense point cloud can be done. Equation (2) formulates this estimation in introducing the GSD in order to attach the value to the object space coordinate system. R denotes the estimated resolution of the dense matching result, which corresponds with the notion of resolution in laser scanning (i.e. distance between two points in the point cloud).

$$R = \frac{D}{P} * GSD \quad (2)$$



## Chapter IV Results and analysis

### IV.1 Sensor calibrations

The calibration was performed for the two sensors integrated within the two UAVs used in this project. Several softwares were used to perform the calibration as to compare the results: Photomodeler, Photoscan, and the Apero module of the Micmac software suite. For the sensor in Albris, the calibration was also performed using PostFlightTerra3D which is a limited version of the software Pix4D. Due to limitations in licencing options, this is only possible to do with the Albris. However, it is also possible to compare the results with the values given by Pix4D.

During the calibration, the only criterion which was not respected was the rotation of the sensor into the portrait mode. The two UAVs are equipped with gimbals which prevents the sensor from deviating from a horizontal position. As a result, the portrait images were not taken. This may eventually generate a correlation between the parameters P1 and P2, which further means that these two values should be deactivated during the calibration calculations.

The values obtained from the different softwares are variable, which shows the instability of the sensors. This may come from the fact that the sensors integrated to the UAVs are small sensors. In the case of the Phantom 3, a small systematic error is noticeable in the value of  $c$  (focal length) and  $x_0$  and  $y_0$  (principal point coordinates). In order to detect this systematic error, the obtained values were averaged and compared to the value given by Pix4D. A difference between 0.1 and 0.2 mm is detected on these 3 parameters. In contrast, for the values of Albris, the difference is only around 0.04 mm.

As regards to the radial distortion, Phantom 3 shows an anomaly. In the case of this comparison, all values are converted into the Photomodeler format, wherein the unbalanced mathematical model is used. Normally in this type of model, the distortion value is either always positive or always negative. However Phantom 3 gave positive and negative values as the radius from the image center increases.

This anomaly may be explained by the statistics given by Photomodeler. Indeed, there is a strong correlation between the K2 and K3 values of up to 96.9%. Furthermore, the standard deviation of the K2 value is very high (1.6 times that of the value itself). (Fraser 2013b) mentioned that for low precision sensors, K3 and eventually K2 may be deactivated. Indeed, the deactivation of these two parameters gave radial distortion values which suit the expected trend better.

On the other hand, Albris gave stable results between the different softwares. The radial distortion curve also gave the characteristics of an unbalanced model.

Some sources of error during the process of calibration:

1. The quality of the sensor: the UAVs used in this project are equipped with small sensors. Phantom 3 has a 6.5x5 mm sensor while Albris is equipped with a slightly larger 10x7.5 mm sensor. These types of sensors are not designed for high precision use and were rather made for visual works. Indeed, the radial distortion value can theoretically reach 40 pixels for Phantom 3 and 90 pixels for Albris (for points located on the image edges).
2. Sensor instability: Being small sensors, their internal geometry is easily changed due to movements or changes in imaging conditions. The photographs were also taken using the auto-focus mode; this gave more instability on the obtained values because each image taken would have a slightly different focal length.
3. Quality of the images: In our case, the calibration was done using coded targets which are detected automatically by Photoscan and Photomodeler. However, the other solutions didn't have this capability of coded target automatic detection. The quality of the image is therefore very important when clicking the points manually. Similarly, the feature matching

which is used to strengthen the quality of the calibration is also influenced by this fact. In the case of the Phantom 3, this factor is limited by the image size of 12 MP. For Albris, noises were present on the images on all datasets. This noise may therefore influence the quality of the calibration.

## IV.2 Preliminary test: the Joséphine Pavilion

A preliminary test were performed on the Josephine Pavilion, a 19<sup>th</sup> century building located inside the Orangerie Park in the city of Strasbourg. The building was photographed using the UAV DJI Phantom 3. The images were taken from an average distance of 8 meters in such way as to cover the four façades. Nadiral images were taken around the object. Being a test project, only several control points were measured on the face by using a total station with the help of the city of Strasbourg. The particularity of this building is its material. The north (back) façade is made from red sandstone, typical of the Alsace region while the south (front) façade is a relatively smooth wall painted in beige, giving little texture.

The back façade was modeled quite nicely, except for several problems where there are vegetations at the left side. However, the front façade suffers from a lot of noises. Note that the point clouds of the windows are good. In his case, the presence of texture on the object becomes an important factor, because the dense matching algorithms depend also on the correlation coefficient. The lack of texture hampers the matching process on the white wall because the algorithm cannot distinguish the different tie points. These points thus became noises. A comparison of dense matching results of the central part of this façade using the employed matching algorithms is shown in Figure IV.1.

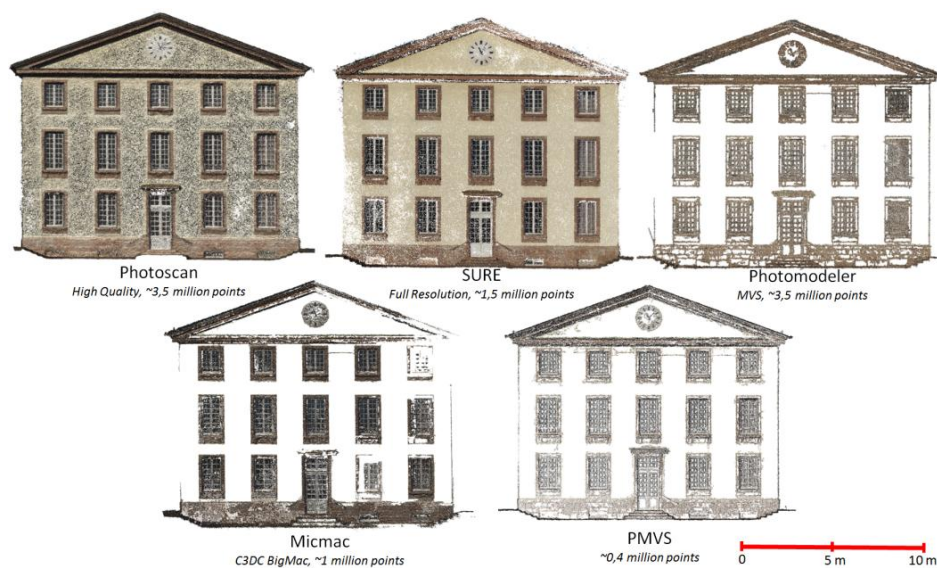


Figure IV.1 Dense matching results of the central front-façade of the Josephine Pavilion, showing point clouds generated by the five dense matching algorithms employed.

Visually, Photoscan managed to retrieve points on the problematic beige wall. However, these points are noisy with up to 15 cm of dispersion on a wall which normally should be flat. Similarly with Photoscan, SURE also generates points on the painted surface with noises. On the contrary, processing on Photomodeler (using its MVS dense matching mode), Micmac, and PMVS detected only a sparse amount of points on this smooth surface.


Several preliminary analyses were taken from this pilot project. The first concerns the importance of image overlap of the object; indeed echoing the need for detailed images with large percentage of overlap mentioned in the existing protocols. A remark was made to acquire controlled oblique images in further projects in order not only to strengthen the image network geometry but also to

better cover hidden parts (window sills, awnings, balcony, etc.). Oblique images will emulate the concept of detailed stereo pairs in a UAV acquisition scenario.

Furthermore, the problem of the object in question's material is also important to note. In the case of the pavilion, a textureless material hinders a proper pixel-by-pixel search for correspondence. Particular strategies should be taken to address this problem. One strategy that can be employed involves changing the resolution of the images used in the dense matching; bearing in mind that in this case a better resolution matching does not necessarily produce a better result. Another involves changing the correlation coefficient threshold to allow more points (which may however be noisy) to be detected.

### IV.3 First case study: the Rohan Palace

The Rohan Palace is a historical landmark of the city of Strasbourg dating to the 18<sup>th</sup> century. Located next to the cathedral, the palace was built for the Cardinal Rohan between 1732 and 1742 and housed several French sovereigns during their visits to Strasbourg. Today it is used by three museums, all managed by the city's administration. In regards to the material, the palace is made of yellow sandstone. For this project, only the central façade overlooking the River Ill was photographed. The dimension of this façade is approximately 14 x 20 meters.



|                                 | Photoscan                                | Pix4D                           | Micmac  | Photomodeler                    |
|---------------------------------|--|---------------------------------|---|---------------------------------|
| <b>Preset name</b>              | Medium                                   | Quarter Resolution              | C3DC MicMac   | N/A                             |
| <b>Input images resampling</b>  | 25%                                      | 25%                             | 25%   | 25%                             |
| <b>Point cloud downsampling</b> | Unknown                                  | 4 ("Optimal")                   | 4   | 2                               |
| <b>Post-matching filtering</b>  | "Aggressive", probably coplanarity based | Coplanarity based, 3 rays/point | Actually pre-matching, based on best master and secondary images (AperoChImSecMM) | Coplanarity based, 3 rays/point |

Figure IV.2. Dense point cloud generation parameters of the four algorithms tested.

In this project, the Sensefly Albris was used to acquire the images. Using its capability to fix camera-object distances, the UAV was flown at a fixed approximate distance of 5 meters from the façade. In addition, 13 control and check points scattered on the façade are measured using a total station using the spatial intersection method in order to be able to assess the precision and accuracy of the results. The 6 control points are placed on the limits of the flight zone following the classical aerial photogrammetry configuration. The remaining 7 points were used as check points, and are scattered evenly on the façade to represent changes of reliefs.

All algorithms succeeded in orienting the images except VisualSFM, which might be linked to the default number of detected tie points. Despite the theoretical GSD of 1 mm, here the precision of the aerotriangulation for all four solutions was on average 9 mm while the check point accuracy was 7 mm. It should be noted that the control and check points used are detail points (window edges, bricks, etc.) and not well defined targets. The precision and accuracy depend therefore on the quality of point marking. This however, was hampered by the noisy quality of the Albris' images. This noise problem has been acknowledged by Sensefly and an improvement of sensor quality is expected sometime soon.



As regards to the dense point cloud, the results as well as matching parameters employed for the four dense matching algorithms are shown by Figure IV.2. The matching settings used in each algorithm correspond to the resampling of the input images to a quarter of their original resolutions. Note that this resolution setting is often employed in dense matching solutions in order to give the users a compromise between quality and processing time. The application of oblique images has effectively covered several difficult places such as the balcony and the lower part of the triglyph or the metope above it. However, the question of image noise still posed a problem. Indeed, a test performed with matching using half resolution images generated a sparser point cloud with many holes. On the contrary, a more complete point cloud was acquired using a lower resolution setting. This problem is most probably caused once again by the correlation coefficient threshold; in the higher resolution setting the algorithm calculates denser points which it assumes are noises and therefore deletes, leaving holes in the resulting point cloud.

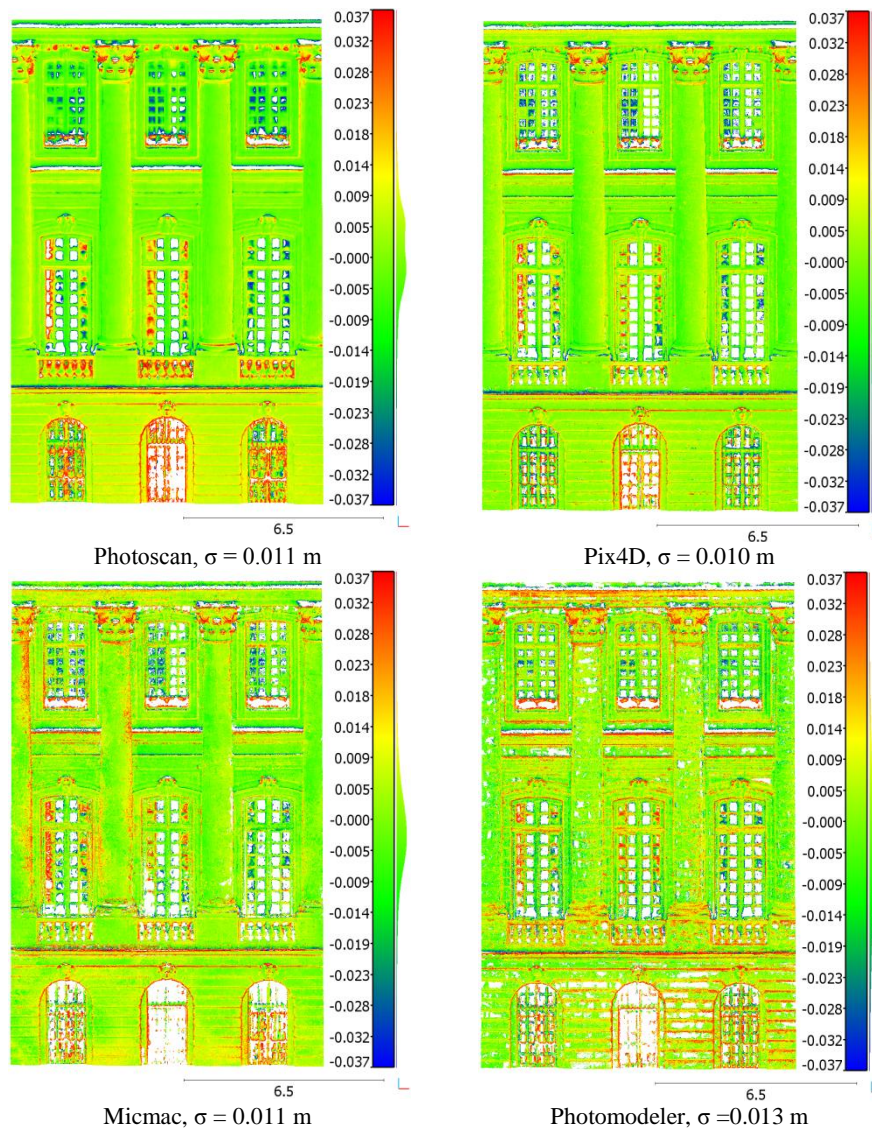


Figure IV.3. Dense matching results analysis using laser scanning data as reference for a common part of the façade of the Rohan Palace.

Furthermore, in order to validate the accuracy of the dense matching results, a terrestrial laser scanning survey was performed on the façade concerned. This was done using a Faro Focus 3D laser scanner and the resulting point cloud has a resolution of about 6 to 8 mm. Evaluation was performed for a common portion of each result of the photogrammetric dense matching using the laser scanner point cloud as reference (see Figure IV.3). All solutions gave standard deviations of around 1 cm compared to the reference. This corresponds more or less to the theoretical resolution of the point cloud at this image pyramidal level of matching (around 1.4 cm).

Larger histogram dispersion is observed in Photomodeler's results, which indicates a noisier point cloud. More holes are also observed in this point cloud. Photoscan and Pix4D gave more homogeneous i.e. less noisy results, with Photoscan detecting slightly more error. In addition, Micmac detects more holes in general compared to Pix4D and Photoscan, which may be related to the default correlation coefficient threshold in its semi-automatic C3DC matching mode.

In Figure IV.4, the cross-section of one of the Corinthian columns is analyzed in more detail. The point cloud generated by Photomodeler presents the most noise, concurrent with the histogram analysis. Micmac's results present a circular trend for the cross-section albeit it is a rather rough, unsmooth representation. On the contrary, Photoscan and to some degree also Pix4D, present an almost smooth circular shaped point cloud profile. This suggests a form of interpolation and/or smoothing performed after the matching process to conform to certain geometric constraints. Furthermore, some solutions had difficulties in detecting points at the junctions where the column and the wall meet. Micmac, Photomodeler, and even the laser scanner (at the right junction) failed to detect points in this zone and therefore leave a hole. It is however interesting to note that both Photoscan and Pix4D still manage to detect points and close the hole in these particularly difficult areas, although at the left junction Photoscan seems to have detected false points behind the column instead. On the other hand, Micmac and Photomodeler were also unable to reconstruct the left junction. However, Photoscan and Photomodeler are both less accurate in this case compared to Micmac and Pix4D.

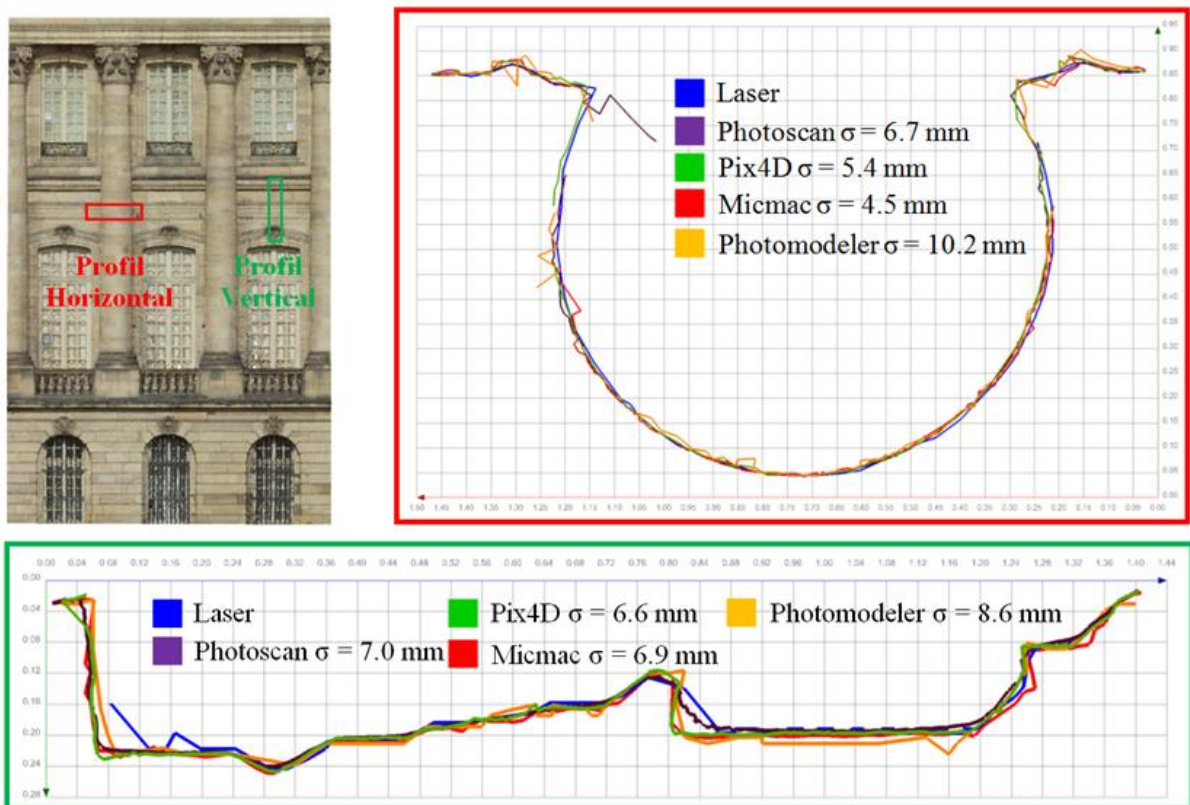


Figure IV.4. A horizontal profile of one of the Corinthian columns (red square) and a vertical one of a part of the wall (green square). The blue lines represent laser scanner measurements.

Figure IV.4 also describes the vertical profile of a portion of a wall generated by the different algorithms. Again, results from Photoscan present a continuous surface which seems to be smoothed to some degree. This phenomenon is however less evident in the Pix4D profile although it can still be observed in a smaller scale. In this regard Pix4D is also a little noisier than Photoscan. Similar to the previous case, Micmac gives a result which follows the trend of the reference with minor noises. Photomodeler gives the noisiest point cloud with errors of up to 1 cm.

#### IV.4 Second case study: the Saint-Pierre-le-Jeune Catholic church

The St-Pierre-le-Jeune Catholic Church was built in Strasbourg during the German era between 1889 and 1889. It is an example of neo-Romanesque architecture crowned by a 50 m high and 19 m wide dome. Both the Sensefly Albris and the DJI Phantom 3 were used to photograph this building. The Albris was used to take high resolution images of the principal façade, while the Phantom 3 was used to complete the rest of the building. In total, 2755 images were taken.

The images from Albris were taken from a distance of 8 m from the façade, which brings its theoretical GSD to 1.4 mm. The object-camera distance for the Phantom 3 was less fixed and ranged between 10 to 15 m. This gives a value of theoretical GSD for the Phantom 3 of around 5 mm in average. Control points were also measured around the church. A polygon network was established around the building which is attached to the French national coordinate system. The photogrammetric control points were measured from these polygon points on the façades of the church.

Due to the presence of some vegetation around the object, several terrestrial photographs were also taken using a standard DSLR camera with an 18 mm lens. The images from Albris were taken from a distance of 8 m from the façade, which brings its theoretical GSD to 1.4 mm. The object-camera distance for the Phantom 3 was less fixed and ranged between 10 to 15 m. This gives a value of theoretical GSD for the Phantom 3 of around 5 mm in average. Control points were also measured around the church. A polygon network was established around the building which is attached to the French national coordinate system. The photogrammetric control points were measured from these polygon points on the façades of the church.

The aerotriangulation gives several interesting points. First of all, the main façade which was photographed using the Albris gives an average precision of 7 mm for the four software solutions used. It should be noted that each control point measurement was performed independently in each software solution. This means that accidental error can be an important factor for the value of precision given by each algorithm. Apart from Photomodeler, the other three solutions also performed re-projections of control points on the images based on a prior approximate orientation using the minimum requirement of three control points. The role of the automatic tie point matching algorithm used by each solution is therefore also important.

It is also interesting to compare this value with the aerotriangulation result from the Rohan Palace data set. The two objects are similar in the sense that both are façades. Here the aerotriangulation result of the St-Pierre data set is of the same order to the one obtained from the Rohan Palace project. However, the object to camera distance in this case is almost two times that of the Rohan Palace. The theoretical GSD of the St-Pierre data set is therefore lower (0.9 mm compared to Rohan's 1.4 mm).

As the focal length of the sensor remains the same between the two projects, a better aerotriangulation result is expected from the Rohan Palace data set. A main cause to this anomaly can be the quality of the images themselves. As previously cited, the UAV Albris used had problems regarding image noise. Indeed, the images on the Rohan data set was noisier than those from the St-Pierre data set, which may be explained by the difference in average object to camera distance. This phenomenon brings into question the interest of taking close range images using this type of UAV, even if they are as close range inspection drones.

The Albris' aerotriangulation precision value is also much higher (up to 9 times higher) than the expected value of around 0.8 mm, based on the average GSD and taking into account pointing error and image quality. The Phantom 3 fared better, with a value of aerotriangulation precision of 14 mm compared to its expected precision of around 5 mm. In any case, using the current flight settings, a centimetric precision is attainable using both UAVs. However, it is worth noting that although



theoretically in photogrammetry the precision can be increased by changing the GSD, in this case it is shown that it is nevertheless limited by the quality of the sensor.

The dense matching process for the principal façade was performed using all four software solutions (Table IV.1), while the rest of the church which was photographed by the Phantom 3 was processed using only Photoscan and Pix4D (Table IV.2). Due to their difference in image resolution, Albris generated a much denser point cloud than Phantom 3 using the same matching configuration. In general, when comparing the dense matching algorithms visually, a similar analysis can be obtained from this data set. Photoscan and Pix4D generated more homogeneous and complete point clouds than Micmac and Photomodeler.

A laser scanning survey was also conducted on the main and south-west façades, in order to compare the results of the dense matching process for both UAVs. The same laser scanner, Faro Focus 3D, was used for this purpose. Four samples, two each from the results of each drone, were analysed (Figure IV.5).

Table IV.1. Dense point cloud generation parameters for Albris images of the St-Pierre data set.

|                                 | Photoscan                                | Pix4D                           | Micmac   | Photomodeler                    |
|---------------------------------|--|---------------------------------|--|---------------------------------|
| <b>Preset name</b>              | Medium                                   | Quarter Resolution              | C3DC MicMac  | N/A                             |
| <b>Input images resampling</b>  | 0.25                                     | 0.25                            | 0.25   | 0.25                            |
| <b>Point cloud downsampling</b> | Unknown                                  | 4("Optimal")                    | 4  | 4 (Level 2)                     |
| <b>Post-matching filtering</b>  | "Aggressive", probably coplanarity-based | Coplanarity-based, 3 rays/point | Pre-matching, based on best master and secondary images (AperoChImSecMM) | Coplanarity-based, 3 rays/point |

Table IV.2. Dense point cloud generation parameters for Phantom 3 images of the St-Pierre data set.

|                                 | Photoscan                                | Pix4D                           |
|---------------------------------|--|---------------------------------|
| <b>Preset name</b>              | High                                     | Half Resolution                 |
| <b>Input images resampling</b>  | 0.5                                      | 0.5                             |
| <b>Point cloud downsampling</b> | Unknown                                  | 4("Optimal")                    |
| <b>Post-matching filtering</b>  | "Aggressive", probably coplanarity-based | Coplanarity-based, 3 rays/point |

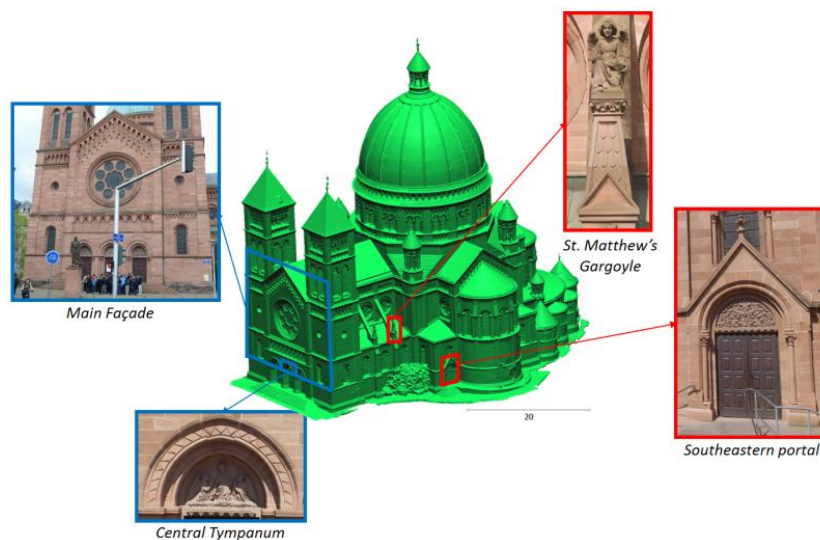


Figure IV.5. 3D meshed model of the St-Pierre data set and samples used to analyse the photogrammetric dense matching results. Blue frames indicate acquisition by Albris, while red indicate acquisition by Phantom 3.

For the main façade, photographed by Albris, all solutions except Photomodeler gave standard deviations of around 1.5 cm (Figure IV.6). Photomodeler is shown to have a higher standard deviation of up to 2.8 cm. This shows a large dispersion in the resulting point cloud generated by Photomodeler, which can be interpreted as an important presence of point cloud noise. Micmac registered a moderate standard deviation, which is without doubt caused by the systematic error observed on the lower part of the façade (the tympanums). A determining factor in this error is the quality of image orientation. Note that the expected theoretical resolution of point clouds generated by these settings is 2.2 cm, so technically all results still fall within the set tolerance.

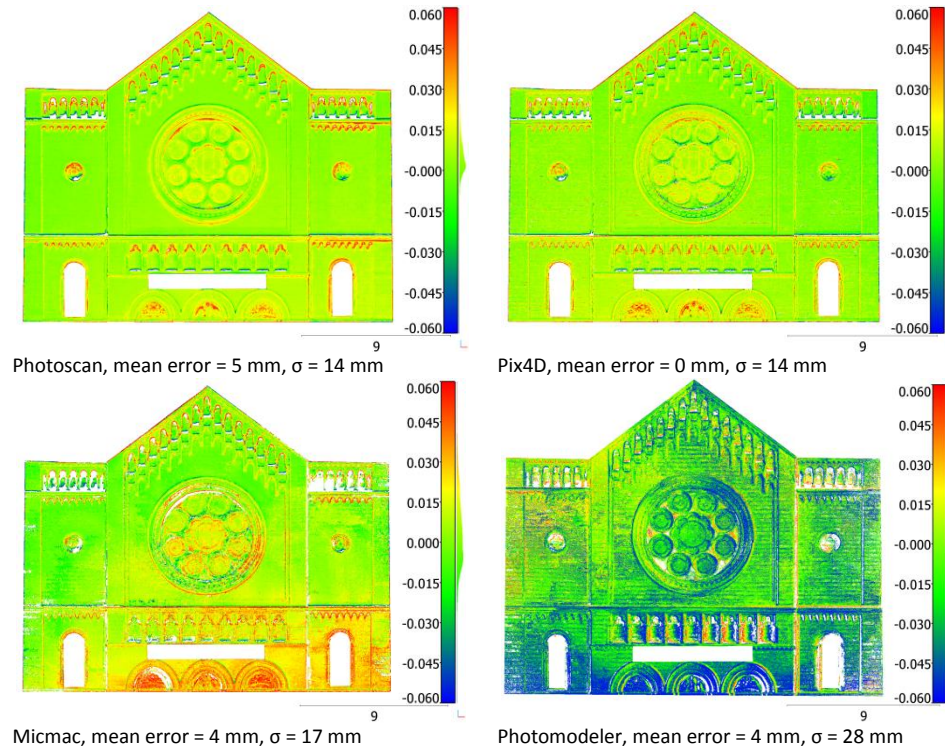


Figure IV.6. Dense matching results analysis for the principal façade of the St-Pierre church.

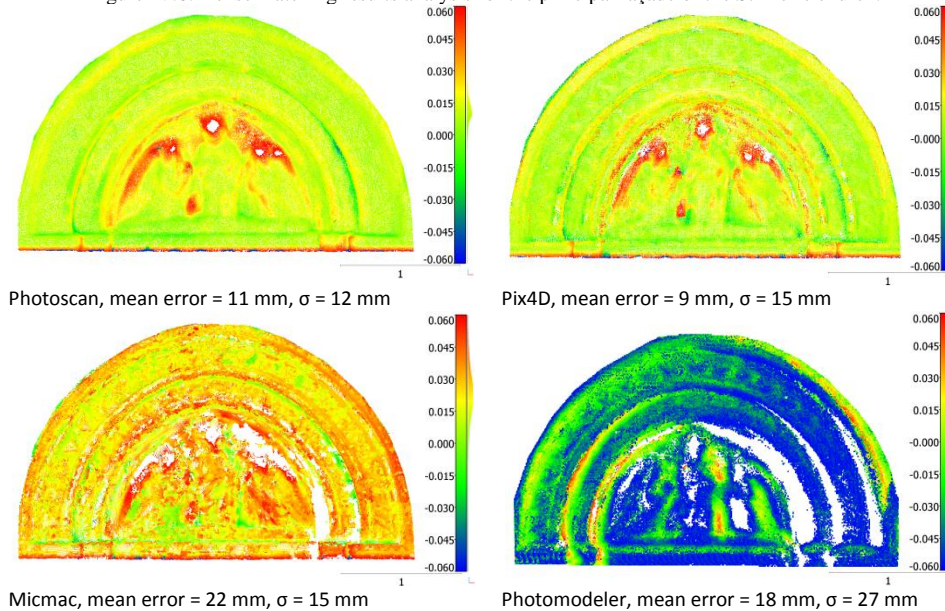


Figure IV.7. Dense matching results analysis for the central tympanum of the St-Pierre church.

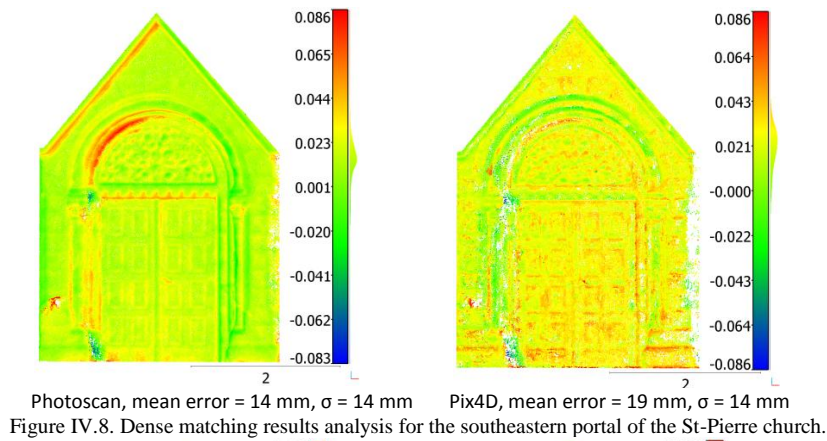


Figure IV.8. Dense matching results analysis for the southeastern portal of the St-Pierre church.

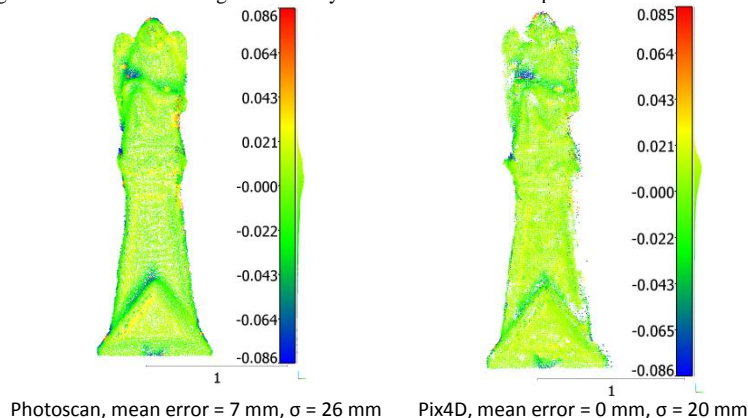


Figure IV.9. Dense matching results analysis for the St. Matthew's gargoyle of the St-Pierre church.

In order to evaluate the result in a smaller scale, the point cloud of the main façade was segmented to extract the central tympanum (Figure IV.7). A slight systematic error amounting to 2 cm is observed in Micmac, while a similar precision as the façade is observed on Photomodeler. Photoscan and Pix4D gave similar results, consistent with the point cloud for the Rohan Palace data set. The mean error in the tympanum is higher than the values for the entire façade for all solutions, which may be explained by the lack of points on the higher parts of the tympanum in the laser scanner point cloud. Photomodeler shows a larger dispersion up to 2.7 cm while the other solutions fall on the average value of 1.3 cm.

Figure IV.8 shows the comparison between the point clouds generated from Phantom 3 images to the laser scanner data. In this analysis, a systematic error is observed on the two results, as shown by the mean error. However, this may be caused by the quality of the reference point cloud, which was obtained from only one station. Furthermore, the portal is also situated at the borders of the laser scanner point cloud, which further explains the existence of systematic error. Both standard deviations are of a similar value of 1.4 cm, which is well within the expected theoretical resolution for this setting of dense matching.

One of the two gargoyles above a flying buttress on the southeastern façade was also analyzed (Figure IV.9). This object is situated right in front of a laser scanning station, which influences the minimal mean error of both software solutions employed. In contrast, the values of the standard deviation are high, up to 2.6 cm. This may be due to the lack of points on the back of the gargoyle in the laser scanner data. The form of the object is also more complex, which implies that in order to obtain better results a dedicated processing should be performed for this level of detail. However, the value of the standard deviation is still within range of the theoretical resolution of the point cloud.



## Chapter V      Conclusions

Several experiments performed during the calibration stage showed that the interior parameters given by the UAV manufacturers are not always stable. Indeed, the calibration takes into account the variations in geometry as well as the stability of the sensor. An anomaly was detected in the radial distortion curve of the DJI Phantom 3. This may be caused by the quality of the sensor itself, which in this case is particularly small. With these types of sensors, the K3 is often correlated to K2; it is therefore wise not to use these parameters for such calibrations. Several experiments have also shown that the calibration parameters given by the manufacturers are not necessarily correct. Pre-project calibration is therefore advised.

As regards to image acquisition, the importance of overlap and the geometric network of the stations is clear in the both case studies. In order to generate a dense point cloud, a large overlap (up to 80%) should be planned. The network geometry is also important to ensure a high precision in the aerotriangulation process. These two problems are usually addressed in terrestrial close range photogrammetry by employing both global and detailed images. In this case where a UAV was used to take images of building façades, the use of oblique images has been very useful.

In order to give a context to the precision obtained in both projects, a theoretical precision was calculated for Albris and Phantom 3. The *a posteriori* precision showed that this theoretical calculation in Albris is much too optimistic, while in the case of the Phantom 3 it is only slightly underestimated. Indeed, during the aerotriangulation stage the image quality plays a very important role in the determination of the precision, more so when no coded targets are used. As seen in the Albris project, noises on the image can reduce the precision up to 15 times worse.

The dense matching of images remains a particular problem to address in a close range photogrammetry project, more so in the presence of noises on the images. The texture of the object plays a very important role, notably for the painted façades such as the case with the Joséphine Pavilion. Therefore, a particular strategy should be envisaged to address these questions depending on the case. In the Palais Rohan dataset, a dense matching using lower resolution images gave a more complete point cloud, although this may not necessarily be more precise. For the Saint-Pierre-le-Jeune dataset the quality of dense matching is strongly related to the computing power and internal memory of the machine. Data management in these cases where the number of images is high becomes very important.

Albris is an interesting UAV for close range inspections. With all of the on-board sensors, this UAV has the potential to become a very powerful inspection tool. This is also thanks to its capability to measure its distance from the photographed object. This function is very useful in close range photogrammetry as it enables the image to keep its GSD virtually constant. However, notwithstanding all of its advantages, this UAV was not ready for use in close range photogrammetry as of the writing of this report. The quality of the sensor needs to be improved to reduce the image noises. According to our observations, an image taken at 5 meters from the object gave the same photogrammetric precision as an image taken at 8 meters. The noise in its turn reduces the quality of the dense matching. Also in regards to its navigation system, many bugs and problems were still apparent during our experiments. DJI Phantom 3 on the other hand, although not especially designed for 3D modeling and close range inspection (as seen by the results of the calibration), is nevertheless a very stable UAV. It has also succeeded to generate a point cloud with centimetric precision without much problem.

In regards to the software solutions tested, Pix4D and Photoscan generated precise point clouds. As already discussed, there is a possibility that these algorithms perform a post-processing in order to give a more homogeneous point cloud. As their algorithms are of a black-box nature, it is difficult to ascertain, nevertheless caution is advised for high-precision projects. Among the four algorithms

tested, Photomodeler is marked with its focus on photogrammetry rather than SfM. Indeed, in several cases Photomodeler managed to give the best aerotriangulation results among the solutions tested. However, the dense matching module of Photomodeler still has several shortcomings compared to other SfM-based software. Finally, Micmac gave precise results both in terms of aerotriangulation and dense matching. Its parameters are also easily modifiable. It is therefore a very useful open-source alternative to the existing commercial solutions.

This Master's thesis has enabled us to perform several experiments on the methods and solutions for the 3D modeling of historical buildings. The use of UAVs is a very interesting aspect of this project, especially in order to assess the quality of its results. The UAV is a perfect solution for the surveying and recording of historical buildings because they are able to take images from points of view which are normally inaccessible to terrestrial techniques. However, several factors remain important and must be paid attention to, including the flight planning, theoretical computation of the GSD and precision, calibration of the sensors, how to fly, project management, etc.

During this project, several analyses were performed on historical buildings in the city of Strasbourg. CIPA explained that such type of documentation is important, because a monument can only be restored and conserved when it is well documented and measured in a repetitive manner and that these information are processed in an organized and structured system.



## References cited in this translation

- Achille, C. et al., 2015. UAV-based photogrammetry and integrated technologies for architectural applications - methodological strategies for the after-quake survey of vertical structures in Mantua (Italy). *Sensors (Switzerland)*, 15(7), pp.15520–15539.
- Afsharnia, H., Azizi, A. & Arefi, H., 2015. Accuracy Improvement By the Least Squares Image Matching Evaluated on the Cartosat-1. *ISPRS - International Archives of the Photogrammetry, Remote Sensing and Spatial Information Sciences*, XL-1/W5, pp.11–14.
- Alidoost, F. & Arefi, H., 2015. An image-based technique for 3D building reconstruction using multi-view UAV images. *ISPRS - International Archives of the Photogrammetry, Remote Sensing and Spatial Information Sciences*, XL-1/W5, pp.43–46.
- Baiocchi, V., Dominici, D. & Mormile, M., 2013. UAV application in post-seismic environment. *ISPRS - International Archives of the Photogrammetry, Remote Sensing and Spatial Information Sciences*, XL-1/W2, pp.21–25.
- Bay, H., Tuytelaars, T. & Van Gool, L., 2006. SURF: Speeded up robust features. *Lecture Notes in Computer Science*, 3951 LNCS, pp.404–417.
- Chiabrando, F., Donadio, E. & Rinaudo, F., 2015. SfM for orthophoto generation: a winning approach for cultural heritage knowledge. *ISPRS - International Archives of the Photogrammetry, Remote Sensing and Spatial Information Sciences*, XL-5/W7(September), pp.91–98.
- Colomina, I. & Molina, P., 2014. Unmanned aerial systems for photogrammetry and remote sensing: A review. *ISPRS Journal of Photogrammetry and Remote Sensing*, 92, pp.79–97.
- DGAC, 2015. Arrêté du 17 décembre 2015 relatif à l'utilisation de l'espace aérien par les aéronefs qui circulent sans personne à bord, France.
- Fraser, C., 2013a. Automatic Camera Calibration in Close Range Photogrammetry. *Photogrammetric Engineering & Remote Sensing*, 79(4), pp.381–388.
- Fraser, C., 2013b. Photogrammetric Camera Component Calibration. In A. Gruen & T. . Huang, eds. *Calibration and Orientation of Cameras in Computer Vision*. Springer Berlin Heidelberg, pp. 95–122.
- Fritsch, D., Cramer, M. & Haala, N., 2013. *UAV im Einsatz für die Datenerfassung beim LGL BW Abschlussbericht*, Stuttgart.
- Furukawa, Y. & Ponce, J., 2009. Accurate, dense, and robust multi-view stereopsis. *IEEE Transactions on Pattern Analysis and Machine Intelligence*, 32(8), pp.1362–1376.
- Grussenmeyer, P., Hanke, K. & Streilein, A., 2002. Architectural Photogrammetry. In M. Kasser & Y. Egels, eds. *Digital Photogrammetry*. Taylor & Francis, pp. pp. 300–339.
- Gülch, E., 1995. Automatic Control Point Measurement. *Photogrammetric Week 1995*, pp.185–196.
- Harris, C. & Stephens, M., 1988. A Combined Corner and Edge Detector. *Proceedings of the Alvey Vision Conference 1988*, pp.147–151. Available at: <http://www.bmva.org/bmvc/1988/avc-88-023.html>.
- Hastedt, H. & Luhmann, T., 2015. Investigations on the Quality of the Interior Orientation and Its Impact in Object Space for UAV Photogrammetry. *ISPRS - International Archives of the Photogrammetry, Remote Sensing and Spatial Information Sciences*, XL-1/W4(August), pp.321–328.
- Hirschmüller, H., 2005. Accurate and efficient stereo processing by semi-global matching and mutual information. *IEEE International Conference on Computer Vision and Pattern Recognition*, 2(2),

pp.807–814.

- Hirschmüller, H., 2011. Semi-Global Matching Motivation, Developments and Applications. *Photogrammetric Week*, (Figure 1), pp.173–184.
- Kemenhub, 2015. *Peraturan Menteri Perhubungan Republik Indonesia tentang Pengendalian Pengoperasian Pesawat Udara Tanpa Awak di Ruang Udara yang Dilayani Indonesia*, Indonesia.
- Kraus, K. & Waldhäusl, P., 1998. *Manuel de photogrammétrie*, Paris: Hermes.
- Lowe, D.G., 2004. Distinctive image features from scale invariant keypoints. *International Journal of Computer Vision*, 60. Available at: <http://portal.acm.org/citation.cfm?id=996342>.
- Morales, A.C., Paez, D. & Arango, C., 2015. Multi-Criteria Analysis of Uavs Regulations in 6 Countries Using the Analytical Hierarchical Process and Expert Knowledge. *ISPRS - International Archives of the Photogrammetry, Remote Sensing and Spatial Information Sciences*, XL-1/W4, pp.175–181. Available at: <http://www.int-arch-photogramm-remote-sens-spatial-inf-sci.net/XL-1-W4/175/2015/>.
- Nex, F. & Remondino, F., 2014. UAV: platforms, regulations, data acquisition and processing. In F. Remondino & S. Campana, eds. *3D Recording and Modelling in Archaeology and Cultural Heritage: Theory and Best Practices*. Oxford, England: Archaeopress, pp. 73–86.
- Nony, N. et al., 2012. Protocols and assisted tools for effective image-based modeling of architectural elements. *Progress in Cultural Heritage Preservation*, 7616 LNCS, pp.432–439.
- Pierrot-Deseilligny, M., De Luca, L. & Remondino, F., 2011. Automated image-based procedures for accurate artifacts 3D modeling and orthoimage generation. *Proceedings of the XXIIIrd International CIPA Symposium*.
- Pierrot-Deseilligny, M. & Paparoditis, N., 2006. A multiresolution and optimization-based image matching approach: An application to surface reconstruction from SPOT5-HRS stereo imagery. *ISPRS - International Archives of the Photogrammetry, Remote Sensing and Spatial Information Sciences*, XXXVI.
- Reich, M., Wiggenhagen, M. & Muhle, D., 2012. Filling the holes - Potential of UAV-based photogrammetric façade modelling. *Tagungsband des 15. 3D-NordOst Workshops der GFaI*.
- Remondino, F. et al., 2013. Dense image matching: Comparisons and analyses. *Proceedings of the Digital Heritage 2013*, 1(Octobre), pp.47–54.
- Remondino, F. et al., 2012. Low-cost and open-source solutions for automated image orientation—a critical overview. *Progress in Cultural Heritage Preservation*, 7616 LNCS, pp.40–54.
- Remondino, F. et al., 2014. State of the art in high density image matching. *The Photogrammetric Record*, 29(146), pp.144–166.
- Remondino, F. et al., 2011. UAV photogrammetry for mapping and 3D modeling - current status and future perspectives. *ISPRS - International Archives of the Photogrammetry, Remote Sensing and Spatial Information Sciences*, XXXVIII(September), pp.25–31.
- Szeliski, R., 2010. *Computer Vision : Algorithms and Applications*, Springer.
- Wenzel, K., Rothmel, M., Fritsch, D., et al., 2013. Image acquisition and model selection for multi-view stereo. *ISPRS - International Archives of the Photogrammetry, Remote Sensing and Spatial Information Sciences*, XL(February), pp.251–258.
- Wenzel, K., Rothmel, M., Haala, N., et al., 2013. SURE – The IfP software for dense image matching. *Photogrammetric Week 2013*, pp.59–70.